Multi-beam laser beacon propagation over lunar distance: comparison of predictions and measurements

A. Biswas*, S. Piazzolla
Jet Propulsion Laboratory, California Institute of Technology, 4800 Oak grove Drive, Pasadena, CA, USA 91109;

ABSTRACT

A multi-beam beacon was transmitted from the Optical Communication Telescope Laboratory (OCTL) located at Table Mountain, CA to the Lunar Laser Space Terminal (LLST), on-board the Lunar Atmospheric Dust and Environment Explorer (LADEE) spacecraft, during NASA's recent Lunar Laser Communication Demonstration (LLCD). The laser beacon (1568±0.1 nm) was square wave modulated and sensed by a LLST quadrant sensor to enable link acquisition and tracking. LLST computed the mean received beacon power and returned 5 kHz sampled power time series over the downlink. Post-processing of the decoded downlink received at OCTL retrieved the uplink power recorded at LLST. The predicted mean irradiance delivered to LLST consistently agreed with the variable beam divergence transmitted from OCTL to within < 1 decibel (dB). Irradiance fluctuations detected at LLST were reconciled with an uplink wave-propagation model derived using independently monitored atmospheric parameters. We report good agreement of the scintillation index and atmospheric coherence time.

Keywords: laser beacon, uplink, scintillation index, atmospheric propagation

1. INTRODUCTION

NASA's Lunar Laser Communication Demonstration (LLCD)[1] hosted by the Lunar Atmospheric Dust Environment Explorer[2] (LADEE) spacecraft was completed in 2013. LLCD set the bar for downlink and uplink difficulty, defined as data-rate × squared distance (Mb/s-AU^2). Additionally, repeated links to the primary ground station located at White Sands, NM and alternate ground stations located near Wrightwood, CA and Tenerife, Spain verified critical aspects such as link handover and interoperability for future operational optical services. One of the alternate ground stations[3] that utilized the Optical Communications Telescope Laboratory (OCTL) located the Table Mountain Facility (TMF) near Wrightwood, CA used a multi-beam uplink laser beacon comprised of six beams for enabling link acquisition and tracking. An indium gallium arsenide (InGaAs) quadrant PIN diode on LLST detected the 1 kHz square wave modulated multi-beam beacon transmitted from OCTL. On-board processing demodulated and low-pass filtered the beacon signal to compute instantaneous power incident on the detector. A 5 kHz sampled beacon power time series telemetered over the downlink to OCTL, extracted by post-processing, contains a record of the incoherently averaged mean uplink power and its fluctuations.

In this paper, measured mean power and its fluctuations caused by atmospheric turbulence, is compared to model based predictions. Data from several links made under diverse link and atmospheric conditions are used. Consistent agreement to within < 1 dB is shown for mean measured and predicted power. Furthermore, a favorable comparison of the measured scintillation index and coherence time with those derived using a wave-propagation model, is presented.

The remainder of this paper is organized as follows. The optical setup used for transmitting and receiving laser signals will be briefly described in Section 2. Section 3 will present the extracted power time series data measured on the LLST and compare it to link budget predictions. Section 4 will present the uplink beacon wave propagation model and compare power fluctuations with predictions. Finally, Section 5 will conclude with brief discussions.

---

* Abhijit.Biswas@jpl.nasa.gov; phone (818)-354-2415; fax (818)-393-6142;

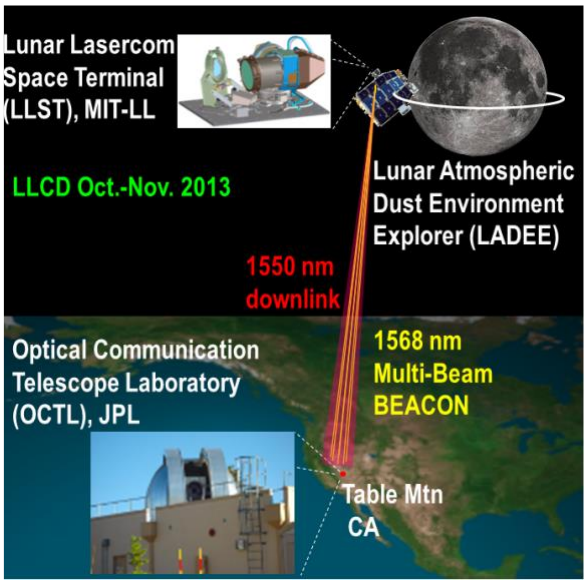

Figure 1. Operational view of the multi-beam laser beacon used to assist LLCD downlink to LLOT.

2. UPLINK BEACON SYSTEM FOR LUNAR LASERCOM OCTL TERMINAL (LLOT)

2.1 LLOT and OCTL at TMF

The 1m aperture diameter OCTL telescope mounted on a fast-tracking elevation over azimuth gimbal is configured with a coudé path to couple light to and from the telescope into a controlled laboratory area. LLOT used OCTL in a bistatic configuration i.e. to transmit the 1568 nm multi-beam beacon while receiving 1550 nm downlink. At least 130 dB optical isolation allowed detecting nanowatts of downlink while transmitting 60W of uplink. Figure 1 provides an operational view of the LLOT used for LLCD.

2.2 Setup

The optical train used in the controlled laboratory area, or coudé room, of the OCTL telescope was presented elsewhere[3,4] and is not repeated. Figure 2 shows a simplified schematic of the uplink optical train for coupling the 6-beam beacon to the telescope. The co-aligned lasers exiting the beam combiner pass through a zoom assembly comprised of a fixed and moving ring of lenses mounted on a linear translation stage. Changing the separation of the lens sets varies the spot size of the individual beams that come to a coincident focus at the telescope coudé focus and propagating through the telescope mirror assembly to a ring of sub-aperture laser spots on the primary. Each beam exits the telescope with divergence proportional to the spot size at the telescope focus. Controlling the spot sizes with the zoom assembly varies the beam divergence launched at the exit of the telescope. On the right of the schematic layout of Figure 2 images of the exiting beams projected on the surface of the dome are shown. The two images represent the two extremities of the zoom assembly, corresponding to 40 μrad and 110 μrad beams exiting the telescope. The six exiting beams propagate through independent atmospheric paths until they overlap in the far field. The launched beams are incoherent relative to each other and uncorrelated atmospheric turbulence induced effects until the beam overlap result in an averaging effect that mitigates fades at the target.

2.3 Beacon monitoring system

Figure 2 shows a pair of pellicle beam splitters that cooperatively split and re-direct a small fraction of the transmitted beacon to a conjugate of the telescope focus on a screen. An imaging camera monitors the aggregate spot size of the overlapping beams. Image processing techniques not only measures the spot size that is proportional to the far-field

divergence but also can detect relative drift between the beams and deviations of the spot centroid from the conjugate focus which will introduce a pointing bias. During operations the beacon monitoring system proved very useful for real-time monitoring of the beam divergence and mis-pointing bias, as well as, providing a means of manually tweaking the alignment that would degrade with time due to mechanical relaxation of mounts sometimes exacerbated by thermal variations in room temperature. Failing to do so prior to the pass resulted in significant pointing bias and poor overlap of the spots at the telescope focus with a reduction in the delivered irradiance at target. Evidence of this will be discussed in Section 3.

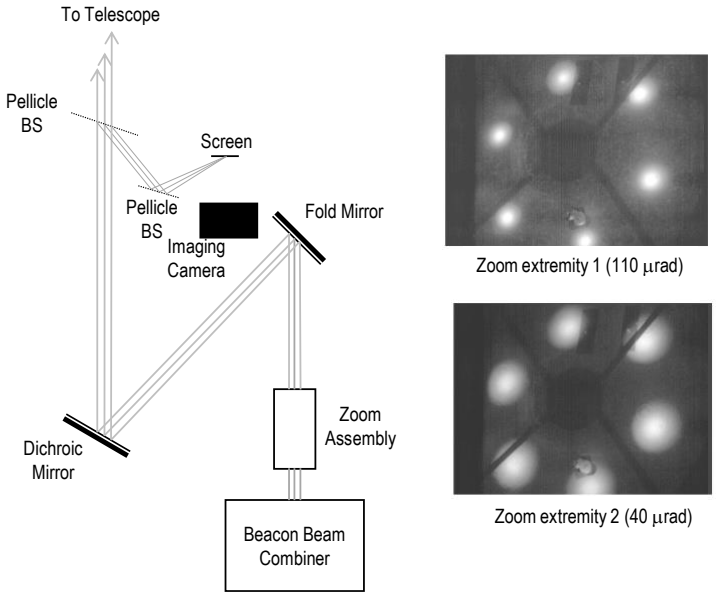

Figure 2: Simplified schematic view of multi-beam uplink beacon. Varying beam divergence (40- 110 μrad) obtained using the zoom assembly could be transmitted; images of spots exiting the telescope aperture and projected on the dome surface at two extremities of the zoom setting are shown on the right. The imaging camera shown in Figure 2 monitored the split fraction of the outgoing beacon lasers at a conjugate of the telescope focus to ensure co-alignment and transmitted beam divergence.

3. UPLINK BEACON DATA

3.1 Measured Data

Figure 3a shows a typical 15-second duration time series of irradiance measured at the LLST on 10/19/2013. The power incident on the InGaAs PIN diode computed on-board the LLST in dBm was converted to irradiance in nW/m^2 using the optical transmission of LLST for the quadrant channel. Observations of fluctuations at two time scales are apparent, the fast and the relatively slow. The red line obtained using a 0.5-second running average smoothing function emphasizes the slow fluctuation. Figure 3b shows the same data with the slow variation normalized out. The analysis presumes that the rapid fluctuations (Figure 3b) are due to atmospheric turbulence. We suggest that pointing jitter causes the slower temporal fluctuations while deferring a more detailed interpretation to future work. Figures 3c and 3d display histograms of the distributions corresponding to Figure 3a and 3b using a longer time series (140 second) of data. The better lognormal fit (red-line) in Figure 3d is consistent with the expected distribution for atmospheric scintillation. The de-trended data series shown in Figure 3b provide means irradiance and normalized variance or scintillation index. We computed power spectral densities of the irradiance time series.

The LLOT uplink budget summarized earlier[3] estimated the uplink irradiance delivered to the LLST. A few passes for with measured uplink irradiance were re-analyzed to estimate the expected uplink irradiance. Ground stored telemetry for the elevation angles, power per beam exiting the telescope and number of beams, monitored beam divergence and

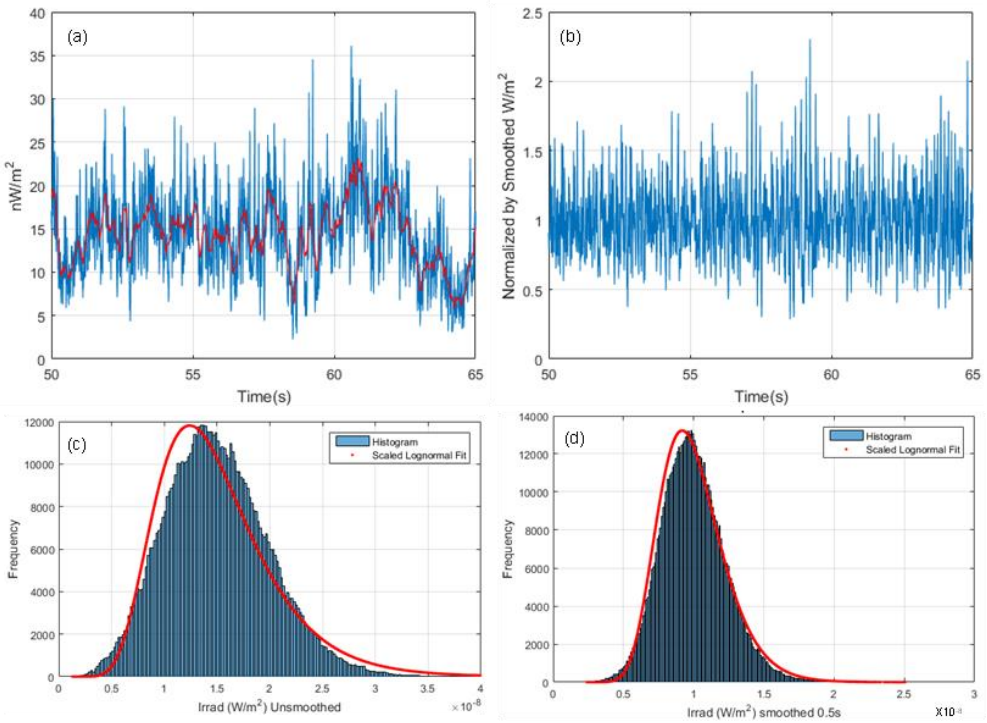

Figure 3: (a) Beacon irradiance measured at LLST (b) Smoothed irradiance data; (c) lognormal fit to histogram of as-received data and (d) lognormal fit histogram of smoothed data.

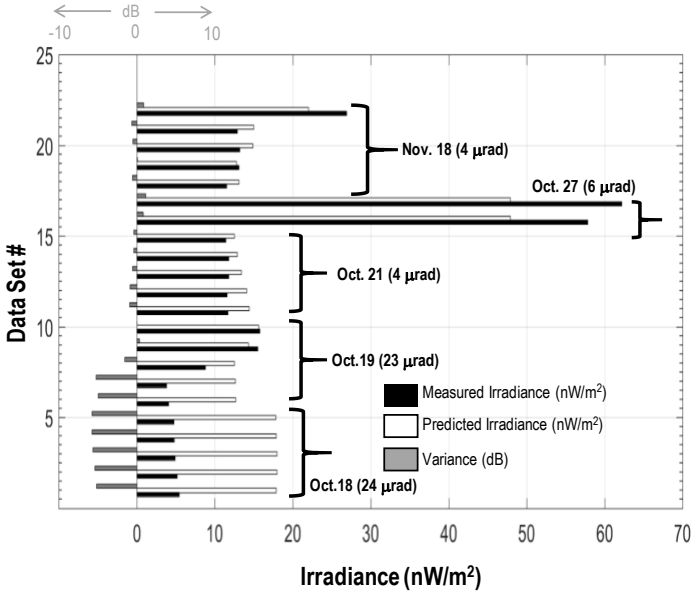

Figure 4: Comparison of measured and estimated irradiance for a number of passes during LLCD.

pointing offset was used to make the estimates of expected irradiance. Actual range retrieved from predicts used during the pass were also used. We assumed a fixed atmospheric transmittance of 0.92 for the expected irradiance estimates.

Figure 4 compares mean measured versus expected irradiance, (black and white bars) along the variance between measurements and estimates in decibels (dB), (gray bars). The annotation shows the dates of the passes and the ground

transmitter pointing bias recorded and stored. Oct. 18 and 19 show large pointing offsets, because the alignment was not refined prior to the link, as was done for all the other data sets shown. Seven out of ten datasets with large pointing offsets displayed large variance of approximately 5-dB. Note that the variance is in spite of assuming large bias in the estimate. This suggests that the bias may have been even larger than what the monitoring system was recording. On the other hand, data sets where the residual bias was relatively small display very good agreement with < 1 dB variance with a few cases of very good agreement. One of the lessons suggested by these results is the importance of monitoring and controlling alignment for transmitting beam width of tens of microradians from ground platforms. As shown the link will probably not break without the monitor and control because of margin in the design however monitor and control can greatly assist in optimizing performance.

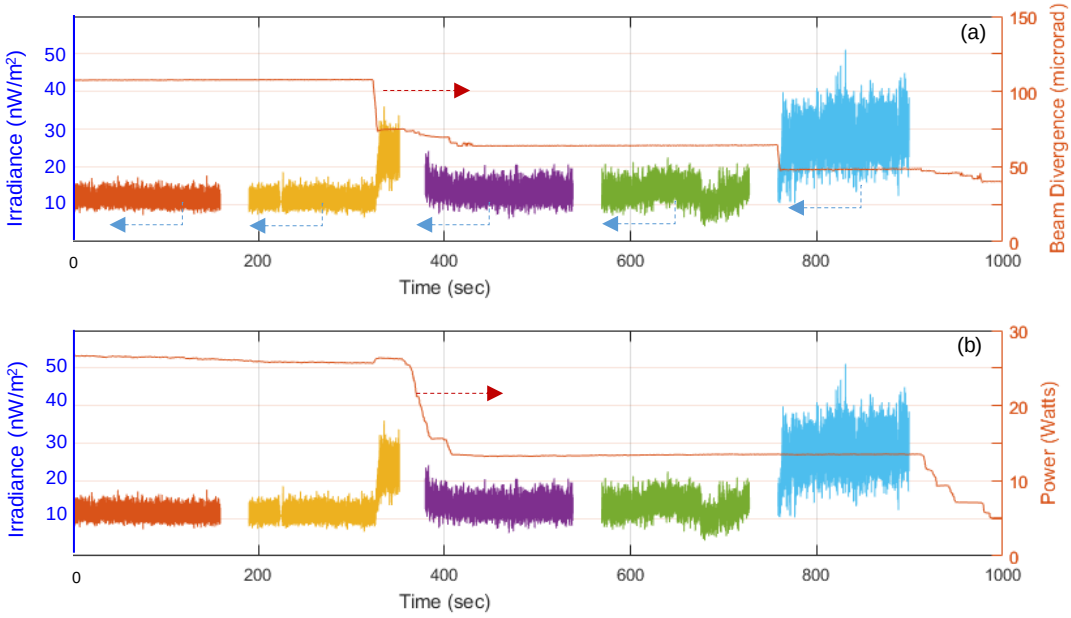

Figure 5: Time series of beacon irradiance along with (a) beam divergence and (b) transmitted power.

Figure 5 shows the measured uplink irradiance as ground transmitter parameters, beam divergence and power are varied. Figure 5a sand 5b show uplink irradiance during a single pass with gaps indicating missing data. As the divergence is reduced (Figure 5a) the irradiance increases and then drops because the power is decreased (Figure 5b). A further reduction of divergence in divergence results in increase in irradiance. The data in Figure 5 represents the last five data sets in Figure 4 where agreement between predictions and measurements was already reported to be -0.6, -0.1, -0.5, -0.7 and 0.8-dB.

Comparison of measured data validates the link analysis for predicting delivered irradiance except for cases when the pointing bias is high. We verified use of the zoom assembly as a means of varying beam divergence to effect the delivered irradiance on target. Other data sets (not shown), where similar variation in divergence was exercised, showed consistent behavior.

4. LLOT BEACON SIMULATION

4.1 Wave Propagation Model

The LLOT multi-beaming uplink system was also simulated using wave optics techniques[5]. Particularly, propagation of the six beams up to the lunar range through the atmosphere was simulated. The overall irradiance at the LLST aperture was obtained by incoherent addition of the six uplink irradiances, producing a time series similar to what was measured during LLCD.

In a wave-optics simulation, a gridded two-dimensional array (or screen) represents an electro-magnetic (EM) field in amplitude and phase. A two dimensional fast Fourier transform[6] (2D FFT) performs the propagation of the EM screen over a distance. Ten intermediate (propagation) steps cover the Earth-to-Moon range in the case of these LLOT simulations. The two dimensional array representing the EM field, propagates from one layer to the next layer in each propagation step. In the atmosphere, propagating optical beams experience phase distortion due to spatial/temporal randomness of the atmosphere's refractive index. To reproduce these phase distortions during a propagation step, an EM field at each screen is modulated by a two dimensional phase screen (or Kolmogorov phase screen)[7]. The phase variation of the Kolmogorov's screen is related to the strength optical turbulence that the EM field experiences in the propagating path.

The simulation produces time series of the signal irradiance at a time step of 1 ms. Translation (shift) of the Kolmogorov's screens in the direction transverse to the direction of the propagation of the optical beam(s) simulates the temporal variation effects of optical turbulence. In each sequence, the amount of spatial shift of the phase screen is given by the product of the corresponding average wind speed (in the given layer) times the update time (1ms).

Overall, the wave-optics simulations we performed are based on input parameters that represents as faithfully as possible the conditions of the optical channel at the time of link; particularly these input parameters are: uplink geometry, beam divergence, wavelength, optical turbulence strength and wind profile in the troposphere.

A dedicated weather station at TMF provided the wind profile, data (ground wind speed and ground wind direction). The ground wind speed is not indicative of the wind speed at higher elevations, where the wind speed can be much different (larger) and at different directions. To model the wind speed at higher elevation, we used the results in Ref. 8. Particularly the reference provides seasonal variability of winds at higher elevation, and in this study, we modeled such a profile based on data collected at Palomar Mountain, CA, the nearest location to Table Mountain. To generate a wind profile for a given simulation, we adopted the high altitude of the wind profile as in Ref. 8 and used the ground level wind speed measured by the weather station for simulation of the LLOT pass. As an example, Figure 6 illustrates an example of wind profile up to 24 Km above ground for a measured ground wind speed of 1m/s measured in the month of November at Table Mountain. The ground level is shifted to 2200 m, corresponding to the altitude of the OCTL telescope, for convenience.

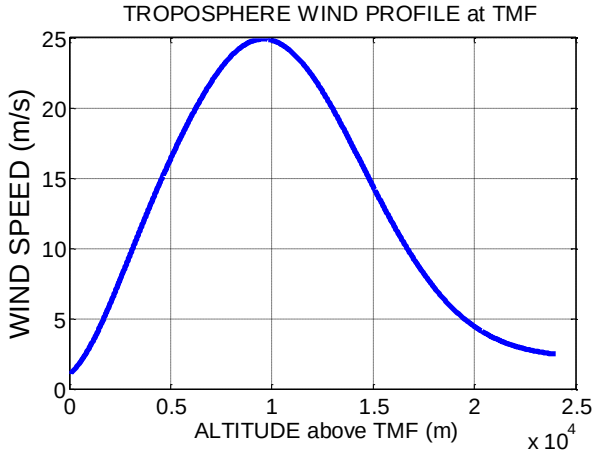

Figure 6: Wind profile at TMF for a ground wind speed of 1 m/s at October. The ground level (altitude = 0) is here at 2200 m above sea level (OCTL elevation).

The strength of optical turbulence along the troposphere is described by the coefficient of the structure function of the refractive index[9], C_n^2 [m $^{-3/2}$]. Real time data of C_n^2 profile coinciding with LLOT passes are not available. Overall, direct measurement along of the troposphere is a complex task, where C_n^2 can experience a large diurnal and seasonal variability, with the largest values of C_n^2 experienced near the ground level. However, to model the C_n^2 profile at TMF, we used profiles based on daytime and nighttime data published in Ref. 10, measured at nearby Rogers Lake, CA during the month of October 2007.
To adopt the turbulence profile in Ref. 10 for LLOT link simulations, we made the following considerations:

1) The profiles shown in the Ref. 10 start around 900ms above sea level (ASL), the altitude of China Lake, while OCTL is 2200m. ASL; therefore data below 2200m were not included in the model. For convenience, we considered the ground level at 2200 m ASL.

2) The profiles in Ref. 10 cover only the troposphere up to 10 Km ASL. To integrate the C_n^2 profile up to elevation, we used a more general model, specifically the Hufnagel-Valley model[11].

3) Additionally a diurnal variation of the turbulence strength was added to the profile in Ref. 10, at the ground layer ($C_n^2(0)$), where the structure constant is the largest. This additional component decreases exponentially with altitude and represents the variable part of our model.

While $C_n^2(0)$ was not directly measured at Table Mountain at the time of the different passes, the overall strength of the optical turbulence was monitored by measuring the atmospheric coherence length[12] or r_0, defined as

$$r_o = [0.423(\frac{2\pi}{\lambda})^2 \int_0^L C_n^2(h)dh]^{-3/5} \quad \text{Eq. (1)}$$

Using the measured value of r_0 at the time of the pass, Eq. 1, and the assumptions on the C_n^2 profile, we were able derive the strength of the optical turbulence value at the ground layer ($C_n^2(0)$) and, therefore, to scale the profile of the turbulence strength ($C_n^2(h)$) for a given pass time.

As an example, Fig. 7 depicts turbulence strength profiles for a measured a measured r_0 = 5 cm at 500nm at zenith for a daytime scenario (blue line) and daytime (red line).

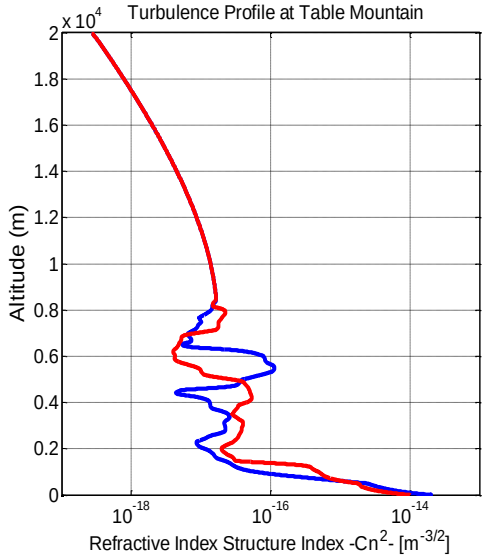

Figure 7: Example of C_n^2 profile for daytime (red) and nighttime (blue) at Table Mountain, CA. The corresponding atmospheric coherence length is 5cm at zenith at 500nm. The ground level is here at 2200 m above sea level (OCTL elevation).

4.2 Simulation Results

The wave-optics simulations replicated as realistically as possible the uplink conditions and geometry at the time of the LLOT pass, including the distribution of the six transmitted beams at the OCTL telescope aperture. The six beams were equally spaced at a distance of 310 mm from the center according to the initial design. Each of the six beams have identical diameter and beam divergence. Of course, the beam diameter varied according the required full beam divergence of the Gaussian beam illuminating LLST.

The elevation angle used for simulation(s) is taken from the recorded telemetry during the pass. One should note that lower elevation with larger apparent atmospheric airmass contributes larger optical turbulence effects. The wave optics simulation produced values of time varying irradiance, for each of the beams, at LLST with a 1 ms update rate. The effective wind considered in the simulation was the transverse component along the direction of the propagation of the beams(s). Because the ground wind speed direction is measured by the weather station, we could scale the ground wind speed component along the transversal direction to the link. However, one should notice that we had no information regarding the direction of the upper level wind speed, therefore we assumed it to be transverse to the uplink direction. The consequence of this assumption is that the overall temporal dynamics (i.e. coherence time) of the final simulation may differ from the measured one.

The incoherent addition of the results for all six beams generated the total irradiance measured at LLST. The fact that each of the six beams experiences distortions from random realizations of the atmospheric paths that are mutually uncorrelated, it is expected that the overall signal fading (respect to that one expected of a single beam) is reduced by a factor N=6, where N is the number of beams used during the uplink. To characterize the signal fading we used the normalized variance of the signal irradiance or scintillation index.

Figure 8 illustrated an example of the propagation of the six beams in three different stages in the path from the primary mirror of OCTL to the Moon. The example depicted corresponds to a realization of the pass on 18 Nov. 2013. The elevation angle was 34º, and full beam divergence of 65 μrad. In Fig. 8a the beams at the exit aperture of OCTl are represented. After propagating 5.8 Km from the telescope, the degradation of the quality of the beams are already evident (Figure 8b), however at this distance the six beams do not fully overlap. The six beams completely overlap at the Moon range, Figure 8c.

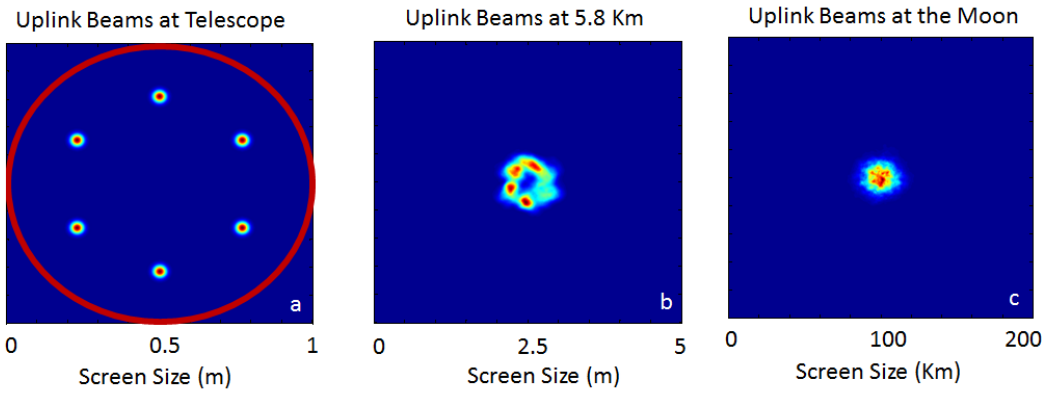

(a) (b) (c)

Figure 8. Pictorial visualization of one realization of the uplink system at the different distance a) Uplink beam(s) at the OCTL primary; b) Uplink beam(s) after 5.8 Km; c) Uplink beam(s) at the Moon.

5. LLOT UPLINK PASS AND SIMULATION RESULTS

Wave-optics simulation results are presented in this section. Particularly, we describe the case of the pass of November 18 2013. The pass took place around 12:03 to 12:22 UTC. At the time of the pass, the ground wind speed varied between 1 to 2.5 m/s and wind direction was between 100 to 130 degree azimuth. The Fried parameter was estimated to be 6cm (at zenith at 500nm).

For this particular pass, two simulations were run with the duration of each being 3 seconds; simulation results were the irradiance time series for each of the propagating beam. Each simulation run represented a given uplink beam divergence used during the actual link. Statistics such as the normalized variance (scintillation index) of each beam and the combination of a number of them were extracted from the time series.

The first simulation is described as it follows:

- Beam Divergence of each beam 65μrad
- Ground Wind Speed transversal to the direction of propagation 0.9 m/s
- Elevation Angle 34 Degree

Figure 9 and 10 illustrate the different signal fading at the Moon represented by the scintillation index. It must be noticed that the average scintillation index for each single beam is 0.177. Particularly, Figure 9 shows the scintillation indices of the possible combinations for two or three uplink beams, and it noticeable how their corresponding values are reduced by (approximately) a factor of 2 and 3. The same reducing law is shown also when 4 or 5 beams are combined, Figure 10, and when all the 6 beams are added together, the corresponding time series of the signal irradiance provide a scintillation index of 0.0277, which is approximately one sixth of initial scintillation index of 0.177, as expected from theory.

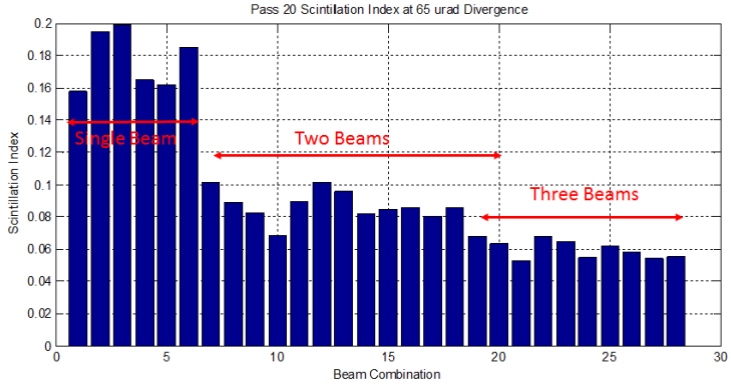

Figure 9. Scintillation Index after simulation for a beam divergence at 65 μrad. Scintillation index is provided for each single beam of the simulation combinations of 2 and 3 beams. Notice, the average scintillation beam for a single beam is 0.177.

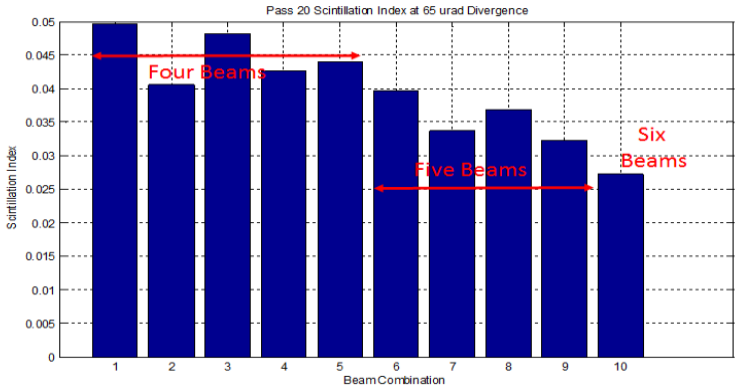

Figure 10. Scintillation Index after simulation for a beam divergence at 65 μrad. Scintillation index is provided combinations of 4, 5, and 6 beams. Notice the scintillation index for the combination of six beams is 0.027.

The second simulation related to the Nov. 18, 2013 pass is described as follows:

- Beam Divergence of Each beam 110 μrad
- Ground Wind Speed 0.9 m/s
- Elevation Angle 37 Degree

In this run, despite the change in beam divergence, a no great change of normalized variance for the signal irradiance was noticed. For the independent single beams the average scintillation index was 0.15, Fig. 11. For the beam constituted by the sum of the six beams at the Moon, the scintillation index was 0.0248, Fig. 12.

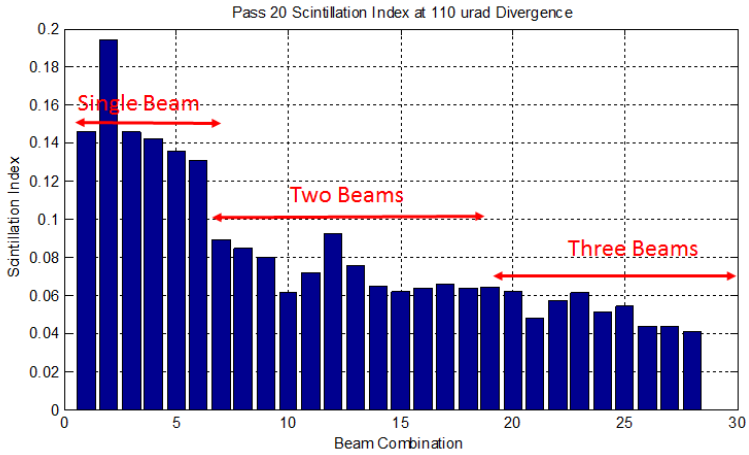

Figure 11: Scintillation Index after simulation for a beam divergence at 110 μrad. Scintillation index is provided for each single beam of the simulation combinations of 2 and 3 beams. Notice the average scintillation beam for a single beam is 0.15.

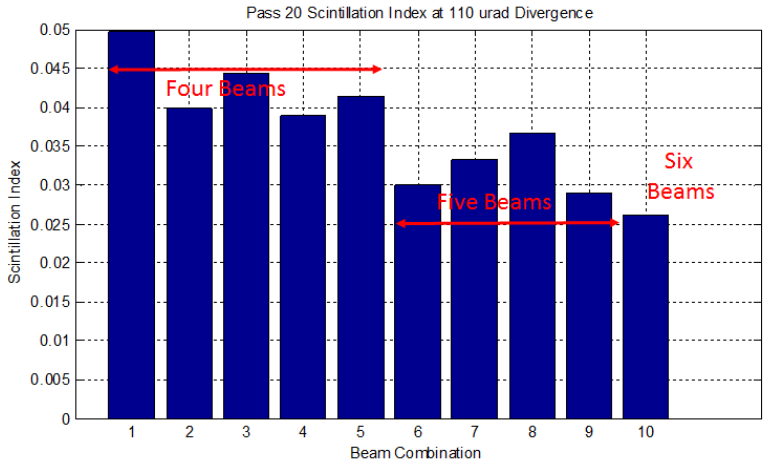

Figure 12: Scintillation Index after simulation for a beam divergence at 110 μrad. Scintillation index is provided combinations of 4, 5, and 6 beams. Notice the scintillation index for the combination of six beams is 0.0248.

Overall, a comparison between simulation results and measurements of the Nov. 18, 2013 pass is provided in Table 1. Generally, the scintillation index values produced by the simulations appear to be larger than those observed/measured at the LADEE terminal. In any case, the overall scintillation index measured and simulated is still pertinent in the range of low scintillation regime, which indicates that the simulation can be considered reliable. Furthermore, our understating indicates that possible discrepancies between simulation and measured data are due to the uncertainties in the assumptions used in the modeling the profile of the strength of the optical turbulence at Table Mountain.

Using data from our simulations, we also compared numbers regarding the coherence time[13] characterizing the fading of the signal irradiance at the flight terminal. The coherence time was calculated with the help of the autocorrelation function of the irradiance time series. Particularly, the coherence time was defined as the time where the autocorrelation function of a given time series drops in value as 1/e. Table 1 compares values of the coherence time of the fading process during the two passes. It can be notices that the simulations produced coherence time values lower that that one observed at the flight terminal for both passes. Again, we believe that uncertainties in the assumption in the modeling of the turbulence profile, and, moreover, uncertainties in modeling the wind profile (wind speed and wind direction above the ground was not directly measured) can be reflected in these numbers. The simulation, however, was able to capture that fact in the case of the 100 μrad beam divergence there was a reduction of the coherence time larger than 50% respect to the case of an illumination of 65 μrad beam divergence.

Table 1

Link	Measured Scintillation Index	Simulation Scintillation Index	Measured Coherence Time (ms)	Simulation Coherence Time (ms)
Pass 20 at 65μrad Divergence	0.018	0.027	22.4	15.9
Pass 20 at 100μrad Divergence	0.011	0.025	9.8	5.0

6. CONCLUSIONS

In conclusion the analysis of the uplink beacon transmitted from OCTL during LLOT showed some good agreement for the analytically predicted mean irradiances and measurements. The benefits of good monitor and control of beacon alignment and divergence is strongly suggested as most mechanical mounts used at ground stations are subject to mechanical drift and relaxation that can be further exacerbated by thermal variations. The use of a zoom assembly for varying beam divergence was verified. The dynamic behavior of the uplink beacon represented by the normalized variance showed very good agreement with simulations, with the simulated scintillation index being slightly higher. For future implementation the simulation can serve as a robust design guide and also provides the added benefit of providing quantitative estimates of scintillation index reduction as a function of the number of beams transmitted. Detector noise effects on the scintillation index measured was not accounted in the analysis presented and is deferred to future follow-on work.

ACKNOWLEDGEMENTS

The authors express their sincere gratitude to Dr. Bryan Robinson of and Dr. Marilyn Semprucci of Lincoln Laboratory, Massachusetts Institute of Technology, for processing and providing the LLOT data that made the analysis presented in this paper possible. The work described was carried out at the Jet Propulsion Laboratory (JPL), California Institute of Technology under contract with the National Aeronautics and Space Administration (NASA).

REFERENCES

[1] Boroson, Don M., Robinson, Bryan S., Murphy, Daniel V., Burianek, Dennis A., Khatri Farzana, Kovalik, Joseph M., Sodnik, Zoran, "Overview and results of the Lunar Laser Communication Demonstration, " SPIE Proceedings, 8971, Free-space Laser Communication and Atmospheric Propagation XXVI, 89710S, 2014.

[2] https://www.nasa.gov/mission_pages/ladee/main/index.html

[3] Biswas, Abhijit, Kovalik, Joseph M., Wright, Malcolm W., Roberts, William T., Cheng, Michael K., Quirk, Kevin J., Srinivasan, Meera, Shaw, Matthew D., Birnbaum, Kevin M., "LLCD Operations using the Optical Communication Telescope Laboratory (OCTL)," Proceedings SPIE, 8971, Free-space Laser Communication and Atmospheric Propagation XXVI, 89710X, 2014.

[4] Biswas, Abhijit, Kovalik, Joseph M., Wright, Malcolm W., Roberts, William T., "Optical Communications Telescope Laboratory (OCTL) Support of Space to Ground Link Demonstrations," SpaceOps Conferences, AIAA 2014-1710, 5-9 May Pasadena, CA, 2014.

[5] Nelson, D. H., Walters, D. L., Mackerrow, E. P., Schmitt M. J., Quick C. R., Porch W. M., Petrin R. R., "Wave Optics Simulation of Atmospheric Turbulence and Reflective Speckle Effects in CO_2 Lidar," Applied Optics, Vol. 39, Issue 12, pp.1857-1871.

[6] Goodman, J, "Introduction to Fourier Optics," W. H. Freeman; December 2004.

[7] Lane, R. G., Glindemann, A. and Dainty, J.C., "Simulation of a Kolmogorov phase screen," Waves in Random Media 2 (1992) 209-224.

[8] Roberts, Lewis C. and Bradford, William L., "Improved models of upper-level wind for several astronomical observatories," Optics Express Vol. 19, Issue 2, pp. 820-837 (2011).

[9] Vernin, J., "'Mechanism of formation of optical turbulence," ASP Conference Proceedings, Vol. 266, Astronomical Society of the Pacific, 2002.

[10] Roadcap, J. R., Tracy, P., "A preliminary comparison of day and night Cn^2 profiles measured by thermosonde," Radio Science, Volume 44, Issue 2 April 2009.

[11] Roggemann, M. C., Welsh, B. M, Hunt, B. R., "Imaging Through Turbulence," Taylor and Francis, 1996.

[12] Fried, D. L., "Optical Resolution Through a Randomly Inhomogeneous Medium for Very Long and Short Exposures," Journal of the Optical Society of America, 56 (10), 1372–1379, 1966

[13] P. Mohana Shankar, *Introduction to Wireless Systems*, John Wiley & Sons, 2002